Optical Engineering

OpticalEngineering.SPIEDigitalLibrary.org

Comparisons between singularities of pseudophase and speckle phase using binary diffusers in optical vortex metrology

Francisco E. Veiras
Ana Laura Vadnjal
Pablo Etchepareborda
Arturo Bianchetti
Alejandro Federico
Guillermo H. Kaufmann

SPIE.

Francisco E. Veiras, Ana Laura Vadnjal, Pablo Etchepareborda, Arturo Bianchetti, Alejandro Federico, Guillermo H. Kaufmann, "Comparisons between singularities of pseudophase and speckle phase using binary diffusers in optical vortex metrology," *Opt. Eng.* **55**(12), 121712 (2016), doi: 10.1117/1.OE.55.12.121712.

Comparisons between singularities of pseudophase and speckle phase using binary diffusers in optical vortex metrology

Francisco E. Veiras,[a,b,*] Ana Laura Vadnjal,[a] Pablo Etchepareborda,[a] Arturo Bianchetti,[a] Alejandro Federico,[a] and Guillermo H. Kaufmann[c]
[a]Instituto Nacional de Tecnología Industrial, Electrónica e Informática, P.O. Box B1650WAB, B1650KNA San Martín, Argentina
[b]Universidad de Buenos Aires, Grupo de Láser, Optica de Materiales y Aplicaciones Electromagnéticas, Departamento de Física, Facultad de Ingeniería, Avenida Paseo Colón 850, Ciudad Autónoma de Buenos Aires, C1063ACV, Argentina
[c]Instituto de Física Rosario (CONICET-UNR), Ocampo y Esmeralda, S2000EZP Rosario, Argentina

Abstract. An analysis based on the comparison between singularities of speckle phase and pseudophase in the practice of optical vortex metrology is carried out by measuring the phase map of the speckle pattern obtained from the transmitted light through binary diffusers. In the characterization of the core structure of both phase singularities, the variation of the measured parameters is produced by means of in-plane linear displacements and rotations of the scattered speckle fields. These fields are addressed by using similar displacements of the binary phase masks recorded in a spatial light modulator (SLM). We complete these comparisons by measuring out-of-plane variations of the core structure parameters. In addition, we verified that the phase map of the transmitted light beam through the binary diffusers recorded in SLMs is actually characterized by a speckle phase with vortices of unitary charge. The presented analysis would be helpful for understanding the scope and limitations of the use of the singularities of speckle phase and pseudophase as position marking, and also for speckle measurement of in-plane rigid-body displacements of binary diffusers dynamically controlled by means of SLMs. [DOI: 10.1117/1.OE.55.12.121712]

Keywords: speckle; optical vortex metrology; phase retrieval; singular optics; spatial light modulator; binary diffuser.

Paper 160370SS received Mar. 11, 2016; accepted for publication Jun. 23, 2016; published online Jul. 12, 2016.

1 Introduction

Optical vortex metrology (OVM) is based on the utility of the pseudophase singularities (PPSs) information of the complex signal obtained from Laguerre–Gauss filtering (LGF) of the intensity of the scattered speckle pattern.[1,2] This complex signal does not introduce new optical information, although it provides a means for in-plane microdisplacement and rotation measurements by using the fact that the PPSs can be detected directly from the recorded intensity of the speckle pattern without using interferometry.[3–5] These PPSs are identified using their core structure parameters such as vorticity, zero-crossing angles, eccentricity, and topological charge. Then, a displacement map of well-characterized phase singularities (PS) from the initial image with its counterpart in the postdisplacement image can be determined. Briefly, the local displacements are measured by identifying the core structure of the PPSs. These are detected by vortex filtering the recorded speckle images corresponding to the initial and postdisplacement states of the tested object. The PPSs are thought as encoders for position marking because they identify a well-defined geometrical point. The pseudophase field has a unique phase structure that includes singularities, which can be seen as topological defects of the wavefronts.[6]

In the practice of OVM, the corresponding identification of the core structure of the PPSs in both states of the object is not always possible. The set of obtained singularities forms clusters with values of the core that are frequently modified by the displacement of the tested object. Moreover, new PS may be created or some of them may disappear. The reader should note that in OVM practices the analysis is carried out based on the object perturbation only and the rest of the experimental variables should be maintained. For these reasons, in order to obtain an effective identification, it is necessary to introduce a merit function, which requires the intervention of an external operator to define the threshold values of the core structure parameters of this function.[2] OVM uses one threshold value that must be set up and is associated with each core structure parameter. Moreover, it needs the introduction of an additional parameter that restricts the searching region of the corresponding pair and also a scale factor, so that a total of six parameters must be set up simultaneously. Typical variations in the experimental conditions require the setting up of the threshold values. In Ref. 5, a function of the threshold values was introduced by using the Poincaré sphere, which is a 3-D vector representation of the core structure. As a consequence, this procedure alleviates the operator's task.

In this work, we present an analysis of the PPSs obtained in the practice of OVM by identifying its correspondence with the measured speckle phase singularities (SPSs), which are generated by the transmitted light through binary diffusers. This analysis is helpful for understanding the scope and limitations of the use of SPSs and PPSs as position markings in optical metrology. In addition, this analysis can

*Address all correspondence to: Francisco E. Veiras, E-mail: fveiras@fi.uba.ar

0091-3286/2016/$25.00 © 2016 SPIE

facilitate the definition of a properly merit function in the practice of OVM. To achieve this analysis, we generate several speckle fields by implementing binary diffusers and synthetic pupils in a liquid crystal used as a spatial light modulator (SLM). For a proper characterization of the core structure parameters of the PPSs, in-plane linear displacements and rotations of the transmitted speckle field are generated by using similar displacements in the binary phase masks that are recorded in the SLM. Using this approach, it is seen that the average speckle size, the statistical independence of the generated speckle fields, and the intensity distributions can be dynamically controlled with high repeatability and without the intervention of movable parts in the optical setup with the consequent benefits.[7] Additionally, we verified that the phase map of the transmitted light beam is actually characterized by a speckle phase with vortices of unitary charge. We emphasized the presentation of this result because speckle fields produced by weak random scattering screens may cause the absence of PS.[8]

Below, we briefly summarize the two-dimensional (2-D) isotropic complex signal representation of a speckle pattern by using LGF and outline the calculation of the parameters of the core structure of a PPS in the obtained complex analytic signal using the Poincaré sphere. The PPSs obtained by the LGF process and the SPSs produced by scattering through the binary diffusers are locally determined by noting that the real and imaginary parts of the corresponding associated complex field are simultaneously null. LG filters provide a useful tool for generating PPSs that are invariant to image linear displacements and rotations. Therefore, this approach can be used for image representation with applications to object tracking and image matching.[1] It is seen that the spatial positions of the PPSs detected by the OVM technique do not correspond with SPSs. In addition, the number of PPSs is a function of the LG filter parameter, while the amount of SPSs is determined by the experimental conditions. However, regarding the variations of the experimental conditions, we show that a subset of PPSs can occupy the same spatial positions as the SPSs by adopting an adequate value of the LG filter parameter. These correspondences between PS pairs are used for purposes of quantitative comparisons. We present measurements obtained from in-plane movements of the speckle fields that are generated by in-plane linear displacements and rotations of the binary phase masks recorded in an SLM. We compare the obtained information about the locations and the core structures corresponding to PPSs and SPSs, and then provide a comprehensive analysis.

2 Laguerre-Gauss Filtering and Representation of the Core Structure of Phase Singularities

Given the original signal intensity distribution of the speckle pattern $I(x,y)$, being (x,y) the spatial coordinates in $\mathbb{R}^2$, the 2-D signal complex representation $\tilde{I}(x,y)$ through an LGF process is described by the relation

$$\tilde{I}(x,y) = \iint_{\mathbb{R}^2} \mathrm{d}f_x \mathrm{d}f_y \, \mathrm{LG}(f_x,f_y)\mathcal{F}[I(x,y)](f_x,f_y)\mathrm{e}^{2\pi i(f_x x+f_y y)}, \tag{1}$$

where $\mathcal{F}[\cdot]$ is the 2-D Fourier transform and $\mathrm{LG}(f_x,f_y) = (f_x+if_y)\exp[-(f_x^2+f_y^2)/\sigma^2]$ is the LG filter of bandwidth parameter σ represented in the spatial frequency domain. Formally, we refer to $\theta(x,y) = \arg[\tilde{I}(x,y)]$ as the pseudophase to distinguish it from the optical phase of the scattered speckle pattern. Equation (1) shows that the pseudophase is not the phase of the optical speckle field. However, an interesting question is whether the PPSs occupy the same location as the SPSs for proper values of the bandwidth parameter σ of the LGF mode. If this were the case, then we could assign a correspondence between both PSs. Then, we could compare and analyze their core structures. Our observation is that OVM is not an interferometric technique. Therefore, the recovery of the SPSs could offer a significant knowledge about the expected variations of the values of the core structure and local positions of the PPSs by means of direct comparisons. This new point of view also considers the use of the core structure of the SPS as optimum encoders for position marking when an interferometric approach is adopted. Note that OVM is based on the fact that PPSs are well-defined geometrical points with defined spatial configuration structure. This structure is a unique fingerprint and, therefore, can be used as an identifiable marking for tracking in the same way as the singular SP obtained by interferometric procedures. Although other comparisons with OVM were carried out by using digital correlation and directional wavelet transforms of speckle pattern images,[9] in our knowledge, OVM has not been compared with the recovery of the SPSs of the scattered light field. We will experimentally demonstrate this correspondence and quantify the characteristic fingerprints of the registered PSs by means of the local elliptic anisotropy of an optical vortex by using the Stokes-like field parameters.

The local elliptic anisotropy of an optical vortex can be analogously described from the Stokes parameters S by calculating the complex gradient vector of the scalar field $\tilde{I}(x,y)$

$$\begin{aligned} &S_0 = |\partial_x\tilde{I}|^2 + |\partial_y\tilde{I}|^2,\ S_1 = |\partial_x\tilde{I}|^2 - |\partial_y\tilde{I}|^2,\\ &S_2 = 2\Re(\partial_x\tilde{I}^*\partial_y\tilde{I}),\ S_3 = 2\Im(\partial_x\tilde{I}^*\partial_y\tilde{I}), \end{aligned} \tag{2}$$

where $\Re$ and $\Im$ are the real and imaginary parts, respectively, and (*) denotes complex conjugation.[10] OVM uses the Stokes parameters obtained from the signal representation $\tilde{I}(x,y)$ generated via the LGF of the intensity of the optical speckle pattern given by Eq. (1). The PPSs are located at the intersections of the two zero-crossing lines in the planes generated by $\Re[\tilde{I}(x,y)] = 0$ and $\Im[\tilde{I}(x,y)] = 0$. The real and imaginary parts are smooth monotonic surfaces, which favor the reconstruction of the local structure of the complex signal around the PPSs by means of the 2-D interpolation of the real and imaginary parts

$$\begin{aligned} &\Re[\tilde{I}(x,y)] = a_r x + b_r y + c_r,\\ &\Im[\tilde{I}(x,y)] = a_i x + b_i y + c_i, \end{aligned} \tag{3}$$

where the coefficients $a_r, b_r, c_r, a_i, b_i, c_i$ are obtained by the least-square method.

The core structure is anisotropic with elliptical contours of amplitude, and the eccentricity of the elliptical contour and zero-crossing angle are parameters adopted as local descriptors. Two additional parameters, named vorticity and topological charge, are also assumed to be invariant to an in-plane rigid-body displacement. A summary of

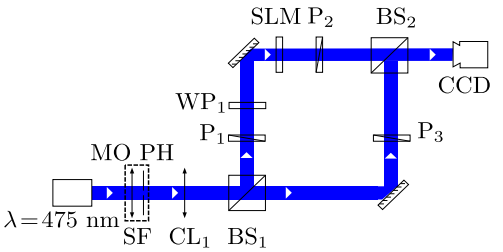

Fig. 1 Experimental setup for the generation and the detection of the speckle fields. 475-nm vertically polarized laser. Spatial filter (SF) formed by a 5X MO and a 50-μm PH. CL_1, collimating lens; BS, beam splitters; polarizers QWP_1, quarter wave plate; M, mirrors; SLM, liquid crystal microdisplay; CCD, and digital camera attached to a computer.

these parameters as a function of the coefficients $a_{r,i}, b_{r,i}$, and $c_{r,i}$ can be found in Ref. 11. Nevertheless, we prefer to work with the Stokes parameters, which can be rewritten from Eq. (2) as

$$S_0 = a_r^2 + b_r^2 + a_i^2 + b_i^2,\ S_1 = a_r^2 + a_i^2 - b_r^2 - b_i^2,$$
$$S_2 = 2(a_r b_r + a_i b_i),\ \ S_3 = 2(a_r b_i - a_i b_r). \tag{4}$$

It follows from Eq. (2) that only three of the Stokes parameters are independent because the relation $S_0^2 = S_1^2 + S_2^2 + S_3^2$ is verified. Therefore, is convenient to define a unit vector with components $\mathbf{s} = (s_1, s_2, s_3) = (S_1, S_2, S_3)/S_0$ on a 3-D sphere surface. For a given core structure of the PS corresponds one point of the sphere and vice versa. OVM is based on finding the appropriate pair matching of the core structures of the PPSs before and after an in-plane rigid-body displacement is introduced. In order to make this possible, a similarity measure with a defined error criterion $\epsilon \geq 0$ for a correct pair identification is given by $|\Delta\mathbf{s}| = |\arccos(\mathbf{s}_{\text{before}} \cdot \mathbf{s}_{\text{after}})| \leq \epsilon$. Once the correct counterpart is identified by the minimum value found with respect to ϵ, the in-plane displacement is estimated from the coordinate change $(\Delta x, \Delta y)$ of the corresponding PPS pair (before and after).

3 Experimental Setup

We measured random wave fields by using a Mach–Zehnder interferometer as depicted in Fig. 1.[12] A vertically polarized light beam from a diode pumped solid state laser of wavelength $\lambda = 475$ nm is expanded and spatially filtered (SF) by means of a 5× microscope objective (MO), a 50-μm pinhole (PH), and a collimating lens (CL1). The main beam is split into two secondary beams (test and reference beam of the interferometer) by means of the beam splitter (BS1). We generate different speckle patterns by placing different transmissive scattering objects in the test beam. The scattering objects were built by using a monochrome display CyberDisplay R 300M LV Kopin Corporation Inc. with an area of 3.3 mm × 2.475 mm, consisting of a regular array of 300 × 225 square pixels of 11 μm and drove by an ad-hoc digital controller. The microdisplay was adapted to work as a phase-mostly SLM by means of a pair of polarizers (P_1 and P_2) and a quarter wave-plate (QWP_1). We follow the procedures of Refs. 13 and 14 to obtain the optimum working parameters of the microdisplay. According to this procedure, the microdisplay is placed between a polarization state generator (PSG) and a polarization state detector (PSD). The best results were obtained for phase-only modulation consisting of a PSG composed by P_1 set to 65.3 deg, a QWP_1 with its fast axis placed horizontally (90 deg) and a PSD composed by a polarizer (P_2) set to 21.4 deg (PSG and PSD angles were measured from X-axis, see Fig. 1). This configuration reached a maximum phase modulation of π rads. The binary diffusers were implemented as described in Ref. 7. Figure 2(a) shows the binary diffuser inside a 100-pixel radius aperture defined in the Ronchi grating phase mask with a period of 2 pixels.

The binary diffuser consists of a pseudorandom structure of macropixels composed by 5 pixels for each side. For the Ronchi grating and the binary diffuser, we employ the same gray levels (GL) codified in 8 bits: $GL_1 = 40$ and $GL_2 = 230$. The two corresponding transmitted intensities for these two GL are similar and the phase difference between them is close to π rads. Therefore, the Ronchi grating phase mask, the synthetic aperture, and the binary diffuser provide a speckle pattern, which minimizes the zero-order beam. Figure 2(b) shows a typical speckle pattern obtained in the described conditions. To this end, we blocked the reference arm of the interferometer.

The intensity measurements were performed with a charge-coupled device (CCD) camera (QIClick-1392 × 1040 pixels) with a pixel size of 6.45 μm × 6.45 μm located far enough (approximately 70 cm from the microdisplay) to obtain a fully developed speckle.[8] As shown in Fig. 2(c), the tilt between the reference and the test arms of the interferometer was adjusted to obtain a fully sampled spatial carrier, which

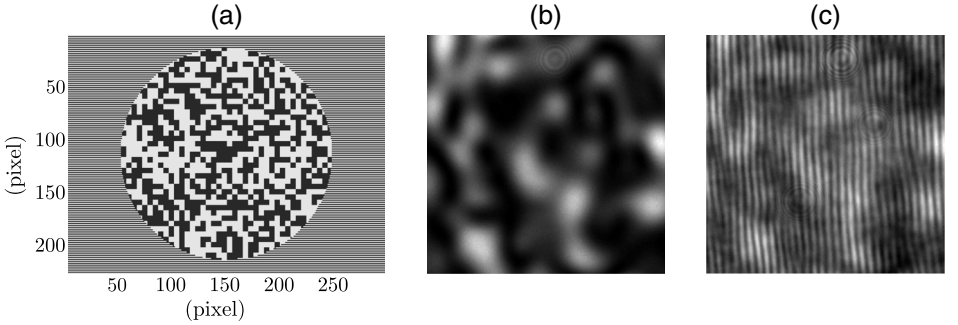

Fig. 2 (a) Mask of the binary random diffuser embedded in a Ronchi diffraction grating. The black pixels correspond to $GL_1 = 40$ and the white pixels correspond to $GL_1 = 230$. The period of the Ronchi diffraction grating is two pixels. (b) Speckle field recorded at the CCD and (c) speckle interferogram, both obtained from (a). The intensity distributions are coded in 12 bits GL from 0 (black) to 4096 (white).

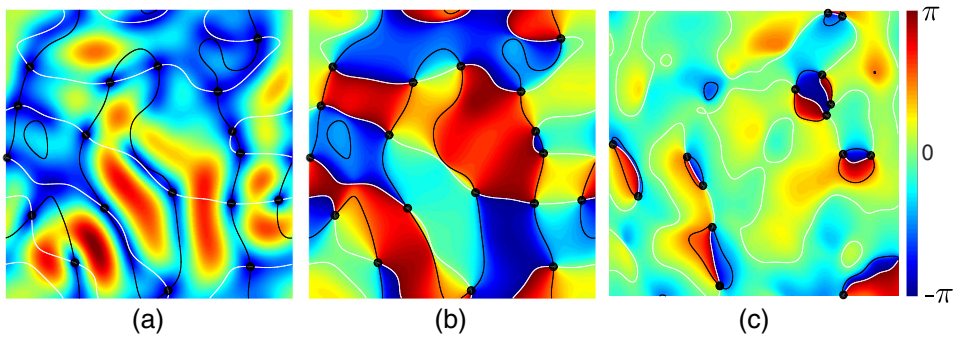

Fig. 3 (a) Amplitude and (b) phase maps obtained from Fig. 2(b) by using Eq. (1) with $\sigma = 0.02$. (c) SP map recovered from the interferogram given in Fig. 2(c). The singular points are denoted with black dots at the zero-crossing obtained by intersections of the real (black) and imaginary (white) lines of each corresponding complex field. The intensity distribution in (a) is coded in levels from 0 (blue) to maximum (red). The phase distributions in (b) and (c) are shown from $-\pi$ (blue) to π (red) color levels.

includes various periods for each speckle grain. An additional polarizer (P_3) was placed in the reference arm in order to match the linear polarization state of the test arm. The binary diffuser is rotated and translated inside the synthetic pupil, which remains fixed along with the Ronchi diffraction grating. This procedure allows an accurate and repeatable control of the in-plane rotations and the linear displacements of the scattered speckle field by means of similar displacements

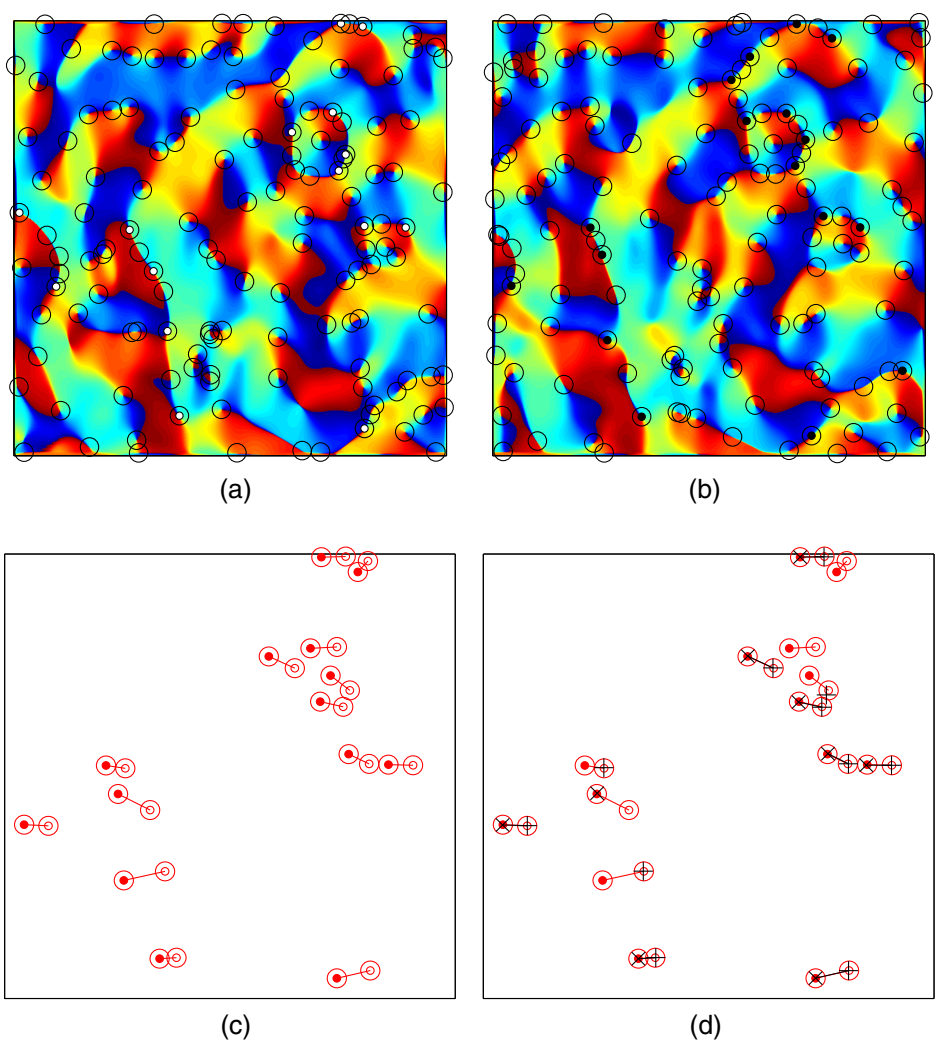

Fig. 4 In-plane linear displacement for a five-pixels horizontal displacement of the binary diffuser shown in Fig. 2(a). (a) and (b) LG pseudophase maps with open circles corresponding to PPSs and small circles corresponding to SPSs before (white) and after (black). (c) Matching of the core structures corresponding to the SPSs: before (small open circles) and after (small red circles). (d) Matching of the core structures of SPSs and their corresponding PPSs pairs: before (plus sign) and after (cross).

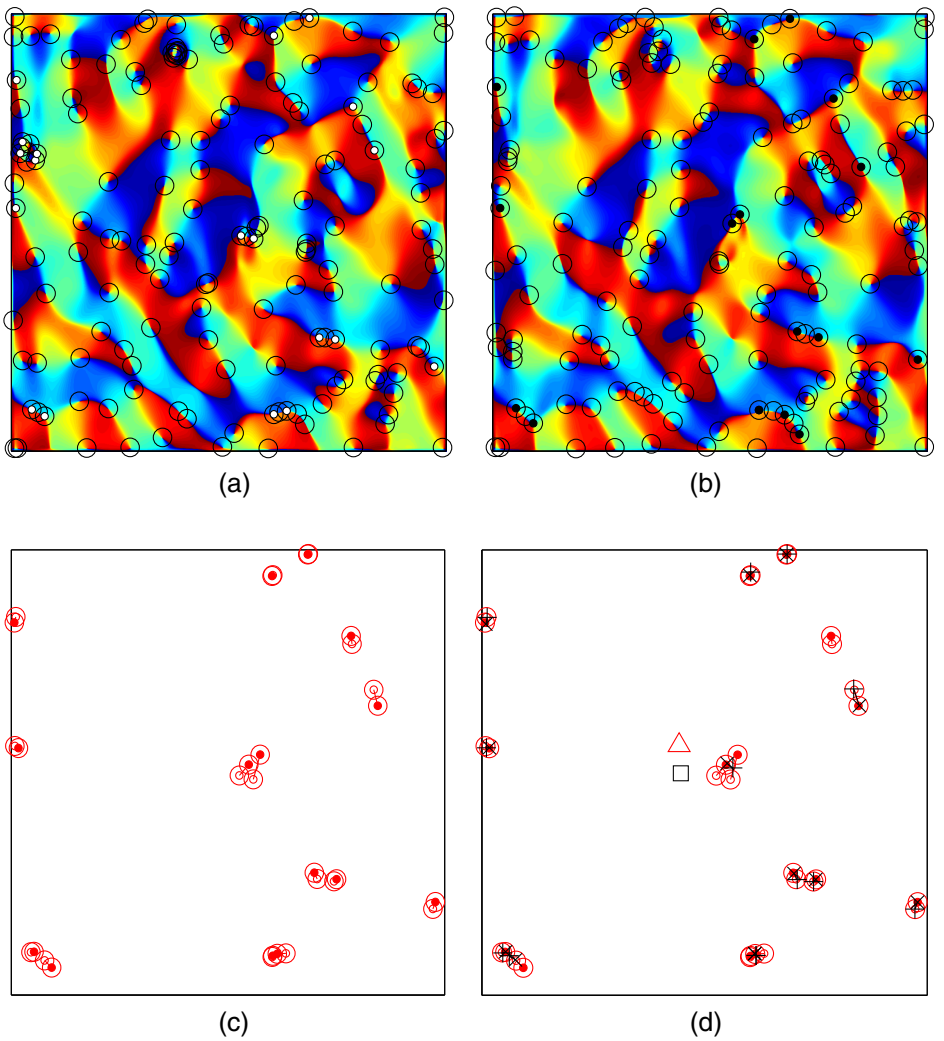

Fig. 5 In-plane rotation for a 1 deg rotation of the binary diffuser shown in Fig. 2(a). (a) and (b) LG pseudophase map with open circles corresponding to PPSs and small circles corresponding to SPSs before (white) and after (black). (c) Matching of the core structures corresponding to the SPSs: before (small open circles) and after (small red circles). (d) Matching of the core structures of SPSs and their corresponding PPSs pairs: before (plus sign) and after (cross). The rotation centers obtained by means of SPSs and PPSs are denoted by a black square and a red triangle, respectively.

introduced in the binary diffuser.[7] We perform several in-plane rotations and linear displacements, and measure the parameters of the core structure of the obtained optical SPSs.

4 Experimental Results

In order to compare the core structure of the PPSs with the optical SPSs, we recovered the scattered speckle phase map by using the Fourier transform method[15] applied to the interferogram shown in Fig. 2(c). The regions of analysis were all cropped to an area of 256×256 pixels. The corresponding PPSs are obtained from Fig. 2(b) by means of Eq. (1) with $\sigma = 0.02$. Figures 3(a) and 3(b) show the amplitude $|\tilde{I}(x,y)|$ and the pseudophase map $\theta(x,y)$ obtained in the LGF process. The PPSs are detected at the intersections (black dots) of the two zero-crossing corresponding to the black and white lines in the interpolated plane generated by $\Re[\tilde{I}(x,y)] = 0$ and $\Im[\tilde{I}(x,y)] = 0$, respectively. By using the same interpolation procedure applied in the recovered complex speckle field, Fig. 3(c) illustrates the obtained speckle phase map with the speckle singularities of unitary charge clearly highlighted. Note that the spatial positions of the PPSs detected by the LGF process do not correspond with those of the scattered speckle pattern.

After the introduction of the in-plane rigid-body displacements, the structure of the binary diffuser shown in Fig. 2(a) does not change. Therefore, we should obtain no variations in the parameters of $\Delta\mathbf{s}$ assigned to the SPSs at the image plane. Equivalently, no speckle intensity variations should be obtained and, as a consequence, no variations in the parameters of $\Delta\mathbf{s}$ assigned to the PPSs should be determined. However, this is not the case in practice. Hence, a comparison between the core structure of the PPSs and the SPSs obtained by an interferometric procedure could offer a better understanding in the scope of using PS as displacement markings. Below, we develop this approach by generating suitable rigid-body displacements and analyze the obtained results.

To produce an in-plane linear displacement, the binary diffuser shown in Fig. 2(a) was horizontally displaced 5 pixels keeping the same binary structure within the synthetic aperture

and neglecting minimum border effects. This mechanism produced a displacement of the scattered speckle field, characterized by I_{before} and I_{after}, from which we obtain the corresponding $\tilde{I}_{\text{before}}$ and $\tilde{I}_{\text{after}}$ by means of the LGF mode. From these filtering images, the pseudophase maps were calculated as $\theta_{\text{before}} = \arg[\tilde{I}_{\text{before}}]$ and $\theta_{\text{after}} = \arg[\tilde{I}_{\text{after}}]$, which are depicted in Figs. 4(a) and 4(b), respectively. By adopting in both cases a value of $\sigma = 0.45$, several PPSs were successfully placed with its SPS pair. These correspondences are depicted in Figs. 4(a) and 4(b) as white (before) and black (after) small circles, respectively. The open circles represent the PPSs obtained by the LGF mode. Figure 4(c) shows the displacement determined by identifying the SPSs recovered by the use of the interferometric procedure. Figure 4(d) summarizes the local displacement identified for both kind of PS, where SPSs and PPSs are distinguished by red and black markings, respectively. Readers should be aware that it is not always possible to find a single value of σ to match all the SPSs with the corresponding PPS pair. Moreover, some singularities appear for a given value of σ, they can disappear for near σ values. However, it is worth noting that certain PPSs remain persistent for greater excursions of σ value. Therefore, a trade-off should be adopted to carry out a comparison. To this end, we fixed a single σ value that best locally matches a subset of PPSs with its corresponding SPS pairs for the displacement before and after. Then, the SPSs are easily traced back by direct inspection, so that the merit function, which defines the maximal excursions in Δs, can be obtained. Note that our analysis is based on the knowledge of the measured speckle phase map, which is not an available information in OVM. By adopting this empirical merit function, we compute the local displacement by using the PPS pairs. Figure 4(d) shows the local linear displacement obtained, which is coincident. These findings also indicate that PPSs and SPSs used as position markings are very sensitive objects when different subtle local variations are present in the field to be measured.

Figure 5 shows the same sequence that was carried out in Fig. 4, but introducing a rotation of 1 deg between before and after conditions from an arbitrary position of the binary mask. This new case is more demanding than an in-plane linear displacement due to the fact that the binary phase

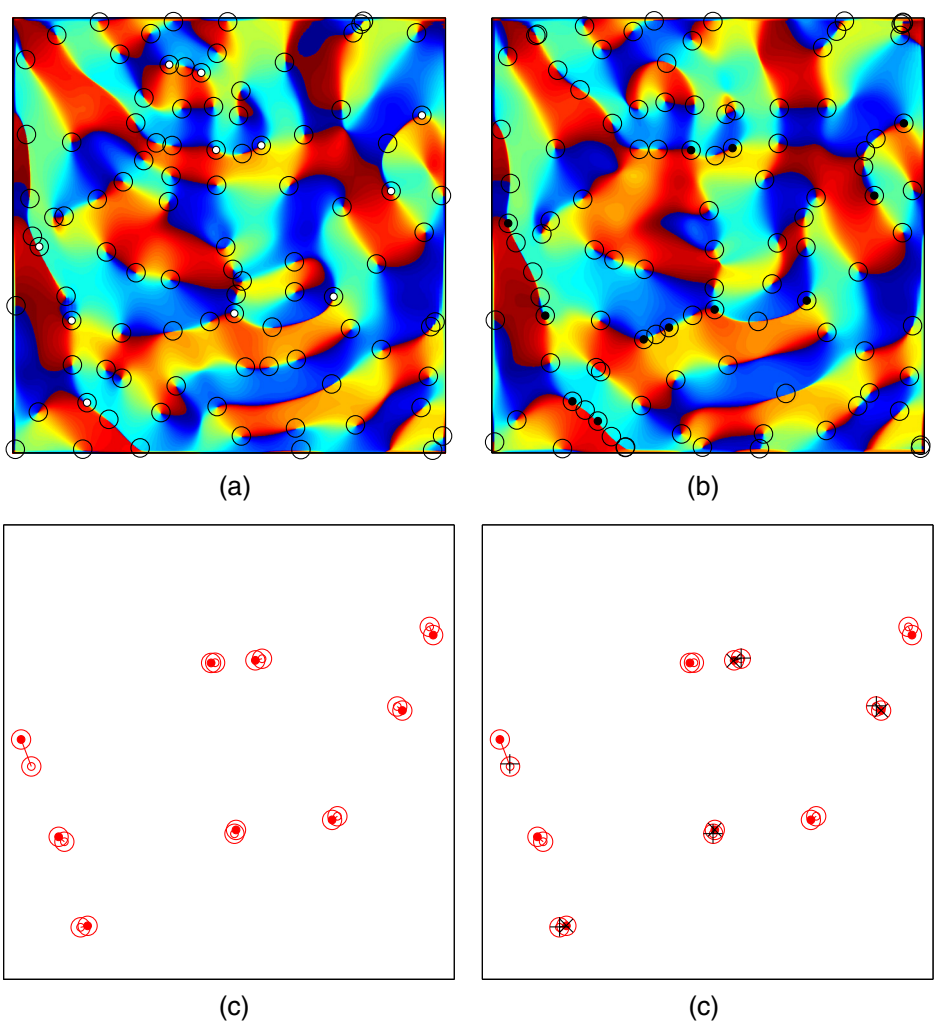

Fig. 6 Out-of-plane linear displacement for a 1-mm linear displacement of the CCD along *Z*-axis (Fig. 1). (a) and (b) LG pseudophase maps with open circles corresponding to PPSs and small circles corresponding to SPSs before (white) and after (black). (c) Matching of the core structures corresponding to the SPSs: before (small open circles) and after (small red circles). (d) Matching of the core structures of SPSs and their corresponding PPSs pairs: before (plus sign) and after (cross).

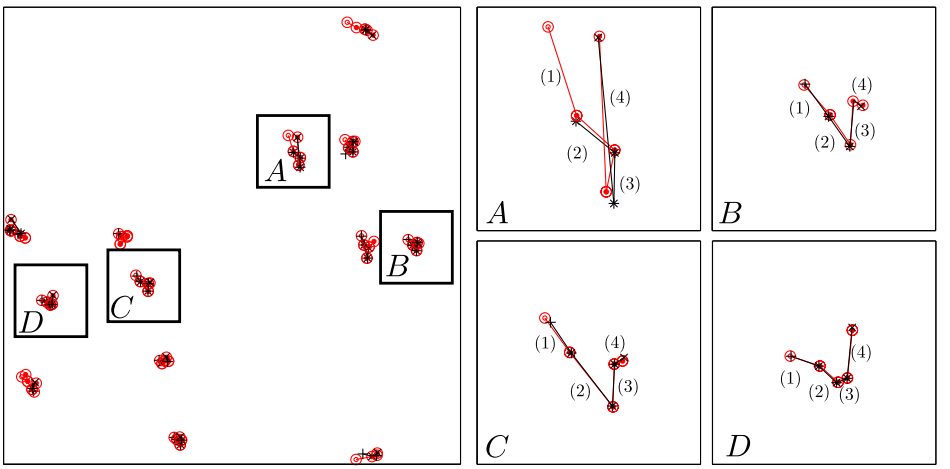

Fig. 7 In-plane trajectory for a sequence of four arbitrary in-plane displacements of the binary diffuser of Fig. 2(a): (1) 1 pixel down and 1 pixel right, (2) 1 pixel down 1 pixel right, (3) 1 pixel up, and (4) 1 pixel up. *A*, *B*, *C*, and *D* trajectories are detailed in the inset. The red and black markings correspond to SPSs and PPSs, respectively with small red open circles (black plus signs) corresponding to singularities before each displacement and small red filled circles (black crosses) corresponding to singularities after each displacement.

mask is affected by a soft pixelating produced by the computer algorithms commonly used for the image rotation. Likewise, we can observe a good identification between PPSs and SPSs as shown in Fig. 5(d). The rotation center was calculated as in Ref. 2. There, a system of equations associated to the bisectors defined by the pairs of singularities is solved by the least-square fitting method. Thus, the pixel location of the rotation center can be estimated with both SPS pairs ($[x, y] = [114.5, 128.5]$) and PPS pairs ($[x, y] = [113.5, 112.4]$).

To gain insight about the stability of the core parameters and the local positions of the PS, we analyzed the correspondences between the PPSs and SPSs when the camera was 1 mm out-of-plane displaced along the optical Z-axis. Figure 6 illustrates the obtained results by using the same procedure described in Figs. 4 and 5. A good identification between PPSs and SPSs can be observed in Fig. 6. Moreover, this last figure shows that the PPSs and SPSs have high persistence in its local positions due to the fact that the CCD was displaced 1 mm along the Z-axis, which is a high excursion value.

As it was previously shown, we have obtained typical results for different kinds of single displacements: in-plane (see Figs. 4 and 5) and out-of-plane (see Fig. 6). We have also identified the SPSs and their corresponding PPSs pair, before and after the introduction of a displacement either in the binary mask of the SLM (in-plane) or in the position of the CCD (out-of-plane). It should be noted that this procedure of pair identification by means of the core structure parameters of singularities can also be employed sequentially. For this reason, we implemented two typical sequences of rigid-body displacements to improve our analysis. In Fig. 7, we show the behavior of the SPSs and PPSs while performing a sequence of linear in-plane displacements. From a given starting point defined as a reference, the phase mask is computationally displaced as follows: (1) 1 pixel down and 1 pixel right, (2) 1 pixel down 1 pixel right, (3) 1 pixel up, and (4) 1 pixel up. We focus on four smaller regions, named *A*, *B*, *C*, and *D*, which show the behavior of both kinds of singularities following the displacements of the binary mask. It is seen that even though the PSs do not rigidly follow the imposed trajectory of the binary mask, both SPSs and PPSs are in a good agreement.

Finally, we describe an out-of-plane linear trajectory by mounting the CCD in a linear stage along the Z-axis. As shown in Fig. 8, the excursions along the Z-axis generate a linear displacement longer than those used previously. However, the XY coordinates of both kinds of singularities remain stable.

To compare the quantitative issues analyzed in Figs. 4–6, Table 1 shows the representative differences of the Stokes parameters obtained before and after the linear displacement, rotation, and Z translation. Table 1 considers $\Delta\mathbf{s} = \mathbf{s}_{\text{before}} - \mathbf{s}_{\text{after}} = (\Delta s_1, \Delta s_2, \Delta s_3)$ for the SPSs and PPSs, which are shown in Figs. 4(d), 5(d), and 6(d). It can be seen that the deviations $\delta(\Delta\mathbf{s})$ were higher for the SPSs than for the PPSs. Note that the mean values $\overline{\Delta\mathbf{s}}$ show important

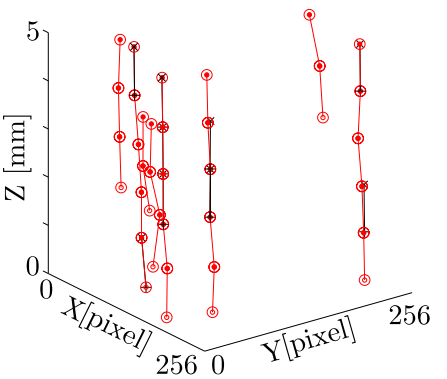

Fig. 8 Out-of-plane trajectory for a sequence of five 1-mm displacements along the Z-axis of the CCD. The red and black markings correspond to SPSs and PPSs, respectively, with small red open circles (black plus signs) corresponding to singularities before each displacement and small red filled circles (black crosses) corresponding to singularities after each displacement.

Table 1 Representative differences of the Stokes parameters obtained for linear displacements and rotation.

Stokes parameter difference	Δs_1		Δs_2		Δs_3	
	$\overline{\Delta s_1}$	$\delta(\Delta s_1)$	$\overline{\Delta s_2}$	$\delta(\Delta s_2)$	$\overline{\Delta s_3}$	$\delta(\Delta s_3)$
			XY-linear displacement			
Speckle phase	−0.1011	0.2939	0.0051	0.2893	−0.1484	0.2909
Pseudophase	−0.1111	0.1849	0.0189	0.1191	0.0661	0.1659
			Rotation			
Speckle phase	0.0006	0.1778	−0.0884	0.3262	0.0302	0.2146
Pseudophase	0.0383	0.1676	0.0460	0.1243	0.0489	0.1813
			Z-linear displacement			
Speckle phase	0.0456	0.2925	−0.0150	0.2745	−0.0491	0.2143
Pseudophase	−0.0900	0.2404	0.0021	0.2221	−0.1283	0.1639

variations from the null value. Therefore, we expect to obtain important deviations in the core structure parameters for before and after position states. We must also mention that we have obtained similar results for measurements performed with different displacements of the binary phase mask, which were not illustrated in this work.

5 Conclusions

We have implemented one technique based on binary diffusers to emulate in-plane rigid-body displacements. We show that the phase of the scattered field corresponds to a speckle phase with vortices of unitary charge. The use of this approach is of great flexibility due to the fact that the obtained intensity distribution can be dynamically controlled with high repeatability by computing phase masks only. Therefore, the average of speckle size can be varied and also generate statistically independent speckle fields without the intervention of movable parts in the optical setup. By using the presented approach, we show that the PSs are very sensitive objects to small local perturbations of the speckle field. Therefore, the applications based on the use of these objects as reference marking should require special cares. Taking into account that OVM uses no information about the speckle phase because it is not a interferometry-based technique, we show that the PPSs can naturally follow the same displacement field as do its SPSs pair. In our opinion, this result is very important in the practice of OVM. However, the PSs can locally have erratic permanency. Therefore, this is an important drawback that cannot be easily addressed and it should be taken into account. Regarding the experimental errors, we observed an important robustness of the core singularities parameters for out-of-plane rigid-body displacements.

Acknowledgments

We thank Ariel Burman for facilitating the crystal display and controller, and the authors from Ref. 7 for fruitful discussions.

References

1. Y. Qiao et al., "A theory of phase singularities for image representation and its applications to object tracking and image matching," *IEEE Trans. Image Process.* **18**, 2153–2166 (2009).
2. W. Wang et al., "Optical vortex metrology based on the core structures of phase singularities in Laguerre–Gauss transform of a speckle pattern," *Opt. Express* **14**(22), 10195–10206 (2006).
3. W. Wang et al., "Pseudophase information from the complex analytic signal of speckle fields and its applications. Part I: microdisplacement observation based on phase-only correlation in the signal domain," *Appl. Opt.* **44**, 4909–4915 (2005).
4. W. Wang et al., "Optical vortex metrology for nanometric speckle displacement measurement," *Opt. Express* **14**, 120–127 (2006).
5. W. Wang et al., "Poincaré sphere representation for the anisotropy of phase singularities and its applications to optical vortex metrology for fluid mechanical analysis," *Opt. Express* **15**(17), 11008–11019 (2007).
6. M. Berry and M. Dennis, "Phase singularities in isotropic random waves," *Proc. R. Soc. A: Math., Phys. Eng. Sci.* **456**(2001), 2059–2079 (2000).
7. L. Cabezas et al., "Speckle fields generated with binary diffusers and synthetic pupils implemented on a spatial light modulator," *Appl. Opt.* **54**, 5691–5696 (2015).
8. X. Chen et al., "Experimental study on the existence and properties of speckle phase vortices in the diffraction region near random surfaces," *Opt. Express* **20**, 17833–17842 (2012).
9. A. L. Vadnjal et al., "Measurement of in-plane displacements using the phase singularities generated by directional wavelet transforms of speckle pattern images," *Appl. Opt.* **52**, 1805–1813 (2013).
10. M. R. Dennis, "Local phase structure of wave dislocation lines: twist and twirl," *J. Opt. A: Pure Appl. Opt.* **6**(5), S202 (2004).
11. W. Wang, S. G. Hanson, and M. Takeda, "Optical vortex metrology," in *Advances in Speckle Metrology and Related Techniques*, G. H. Kaufmann, Ed., Chapter 5, pp. 207–238, Oxford University Press, Wiley-VGH (2011).
12. W. Wang et al., "Experimental investigation of local properties and statistics of optical vortices in random wave fields," *Phys. Rev. Lett.* **94**, 103902 (2005).
13. I. Moreno et al., "Jones matrix method for predicting and optimizing the optical modulation properties of a liquid-crystal display," *J. Appl. Phys.* **94**(6), 3697–3702 (2003).
14. B. Ma et al., "Prediction of optical modulation properties of twisted-nematic liquid-crystal display by improved measurement of Jones matrix," *J. Appl. Phys.* **107**(7), 073107 (2010).
15. M. Takeda, H. Ina, and S. Kobayashi, "Fourier-transform method of fringe-pattern analysis for computer-based topography and interferometry," *J. Opt. Soc. Am.* **72**, 156–160 (1982).

Francisco E. Veiras graduated as an electronics engineer in 2008 and received his PhD in 2013 from the Universidad de Buenos Aires (UBA), Argentina. He is currently a teaching assistant at UBA, and a CONICET postdoctoral researcher at GLOmAe. His current projects are centered around the research and development of polarization control devices and crystal optics, interferometry, and

optical techniques for inspection and detection in micro- and nanosystems. He is a member of SPIE and OSA.

Ana Laura Vadnjal is a PhD student and works at the Instituto Nacional de Tecnologa Industrial (INTI) with a doctoral grant from CONICET. She received her electronic engineering degree from UBA in 2011. She has been a teaching assistant at the Institute of Biomedical Engineering, UBA, since 2008. Her current research interests include signal processing and optical metrology techniques involving speckle patterns.

Pablo Etchepareborda received his PhD in engineering in 2016 from UBA. He is an electronics engineer at UBA. He has been a teaching assistant with the Electronics Department, UBA, since 2008. He has been working in the Optical and Photonics Techniques Laboratory, INTI, since 2009. Since 2016, he has been doing his postdoctoral work with a grant from CONICET. His research interests include optical metrology, image processing, and speckle interferometry techniques.

Arturo Bianchetti graduated as a telecommunications engineer at the Universidad Nacional de Río Cuarto in 2005. In 2012, he received his MSc degree in optoelectronics from UBA, where he is currently a PhD student and a teaching assistant. He has been working in the Optics and Photonics Laboratory, INTI, since 2012. His current research interests include optical metrology and whispering gallery mode microresonators and microfluidics.

Alejandro Federico received his doctorate degree in physical science from UBA. He is with INTI, Buenos Aires, Argentina. His interest is in the development of optical systems, algorithms, and mathematical tools for the advanced processing of optical signals and images for solving inverse problems raised by novel modalities in the field of optical metrology. He works on research and application-oriented projects in tight collaboration with researchers specialized in other branches of the science.

Guillermo H. Kaufmann received his DSc degree in physics in 1978 from UBA. He is currently a professor at the Universidad Nacional de Rosario and a chief scientist of CONICET. He heads the Optical Metrology Laboratory, Physics Institute of Rosario. He has edited 1 book and authored 3 book chapters and more than 150 scientific papers published in refereed journals and conference proceedings. He is a fellow of SPIE and the Optical Society of America.